Modelling, Measurement and Control B
Vol. 87, No. 1, March, 2018, pp. 36-41
Journal homepage: http://iieta.org/Journals/MMC/MMC_B

Impact of flexible blades on the vertical axis tidal turbine performances

Nouredine Drias[1], Mohamed T. Bouzaher[1,2*], Djemoui lalmi[2], Belhi Guerira[1], Derfouf Semch-Eddine[1]

[1] Département de Génie Mécanique, Université de Biskra, Biskra 07000, Algeria
[2] Unit of Applied Research in Renewable Energy, BP 88, Garat Ettaam, Ghardaïa, Algeria

Corresponding Author Email: mohamedbouzaher222@gmail.com

https://doi.org/10.18280/mmc_b.870106

Received: 30 January 2018
Accepted: 17 April 2018

Keywords:
lift force, vertical axis tidal turbine, camber deformable blades, energy extraction

ABSTRACT

Previous research on the vertical axis turbines efficiency has used blades with a typical static camber to improve the turbines efficiency. Typically, the static camber increases the drag force, which affects negatively the optimal harvesting of energy. The present study proposes deformable blades that change their shape relative to their angular position. The new blade shape is achieved by deforming the airfoil camber line via a sinusoidal rounded arc. The computed results show that the present type of deformation involves two typical flow control mechanisms. Firstly, a leading edge control that alters the flow angle of attacks and therefore the leading edge vortex (LEV) time of growth. Secondly, this type of deformation comprises a trailing edge control that affects the physical size and strength of the LEV. The lift force can be effectively increased. As a main result, the turbine power coefficient appears to be higher by about 20% for the optimal operating conditions.

1. INTRODUCTION

One of the challenges related to the turbines with rotating blades is in realizing an optimal blade shape that is required for the optimal energy harvesting. Flexible blades appear as an appropriate solution for an efficient control of such complex flow environments. In fact, they are able to modify their interactions with the surrounding fluid, which can improve the overall aerodynamics performances.

The deformation can be performed passively where no input power is required to deform the structure. This method consists in the use of flexible materials, where their stiffness and damping are keys parameters. The advantage of these methods is that they do not require any power input to maintain a prescribed motion. Simply, it is necessary to choose correctly the flexible material relative to the anticipated objective. In some engineering applications, the preferred shape is not confidently achieved with passive deformation; in such cases, it is preferable to use active deformation. In these methods, an internal mechanism is integrated inside the deformable structure to obtain the anticipated shape. Despite the need of an input power to deform the blade, these methods show a significant improvement in the efficiency [8].

Several computational and experimental studies have confirmed that the efficiency improvement is related directly to the leading edge vortex (LEV) stability. [2, 3, 7, 18, 19]. Both span-wise and chord-wise flexibility can support the LEV control. To improve the overall propulsive efficiency, Heathcote outlined that a judicious span-wise deformation can increase the thrust with an acceptable input power, the LEV size increased dramatically in the case of flexible wings. This point is confirmed computationally by Beem for a flexible ray with an altered leading edge. Changing the leading edge shape demonstrates an improved propulsive efficiency.

For an airfoil having a plunging motion (vertical sinusoidal motion), Miao et al. [15] investigated the airfoil active deformation effect on the flow structure interaction and therefore on the aerodynamic forces behavior. Results indicated that the airfoil deflection affects advantageously the propulsive efficiency.

Jie et al. [10] examined the influence of a passively deformable flexible tail linked to an airfoil flying near the ground. This bio-inspired model shows an aptitude to enhance lift and reduce drag, which produces an improved aerodynamic performance. A flexible flapping tidal generator is investigated by Liu et al. [11]. It is seen that the flexible airfoil is able to modify the classical behavior of the LEV by changing the flow angle of incidence and therefore altering the pressure gradients on airfoil surface.

For the horizontal axis turbine, the concept of flexibility has indicated a great potential to boost lift force and to improve the turbine performance [9, 12-13]. To improve the vertical axis wind turbine efficiency, Ying [20] proposed an adaptive blade that changes its shape relative to the pressure distribution over its surface. It is seen that when the turbine operates at low tip speed ratio, the deformable blades affect positively the turbine output power; however, near the optimal operating range, they appear to have a negligible effect.

For a vertical axis tidal turbine, Liu et al. (2015) addressed the effect of a passively deformable flexible blade on the turbine efficiency. The Results indicate that for high-energy extraction, it is preferable to use less flexible blades. Hoke et al. [8] demonstrated that the concept of active camber deformation could successfully improve the efficiency of energy extraction.

The present paper proposes an actively deformable flexible blade to improve the vertical axis tidal turbine efficiency. To the best of the authors' knowledge, the major difference between the present work and our relevant works [4-5] is the blade deformation mode. The effects of flexible trailing edge and flexible leading edge are exposed in the previous works where the present work is devoted to highlight the camber

deformation effects.

2. POWER EXTRACTION AND FLEXIBLE TURBINE EFFICIENCY

Vertical axis tidal turbine can generate a power P given as:

$$P = \sum_i M_i . \omega \quad (1)$$

where i is the number of blades, ω denotes the turbine angular velocity and M_i represents the moment relative to the turbine center of blade-i

The turbine overall moment is given as:

$$M = \sum_i M_i \quad (2)$$

The power coefficient CP is given by:

$$CP = \frac{P}{1/2\rho U^3 A} \quad (3)$$

where P is the generated power, ρ is the fluid density,U is the incoming flow velocity and A is the rotor swept area.

The blade's moment coefficient C_m is defined as:

$$C_m = \frac{M}{1/2\rho A R U^2} \quad (4)$$

where M represents the rotor torque and A is the rotor swept area.

The tip speed ratio is defined as the ratio between the tangential velocity of the blade's tip and the incoming flow velocity:

$$\lambda = \frac{\omega R}{U} \quad (5)$$

where R is the turbine radius.

To compute the energy consumed by the deformable blades, the turbine efficiency is defined as:

$$\eta = \frac{CP}{CPi} \quad (6)$$

where CPi is the power input coefficient given as:

$$CPi = \frac{Pi}{1/2\rho U^3 D} \quad (7)$$

The power input represents the integration of the pressure and the viscous forces on the foil surface. This power may have a positive value if the pressure gradient assists the deformation or a negative value when the pressure obstructs the prescribed deformation.

$$Pi = \frac{1}{T}\int_0^T \oint F(x,t).\frac{\partial h(x,t)}{\partial t} dldt + \frac{1}{T}\int_0^T \oint F(y,t).\frac{\partial h(y,t)}{\partial t} dldt \quad (8)$$

where T is the cycle, $F(x,t)$ and $F(y,t)$ are the forces components acting on the foil surface respectively in x and y directions. $\partial h(x,t)$ is the instantaneous airfoil position along the x axis and $\partial h(y,t)$ Instantaneous airfoil position along the y axis. dl is the elementary length along the blade surface.

Fig.1 displays the change in velocities and forces acting on the blade during the turbine rotation

The flow incidence angle appears as a function of the azimuthal angle θ and the tip speed ratio λ:

$$\alpha = tan^{-1}\left(\frac{sin\theta}{cos\theta+\lambda}\right) \quad (9)$$

The incoming flow relative velocity W is given as:

$$W = U\sqrt{1 + 2\lambda\, cos\theta + \lambda^2} \quad (10)$$

The lift and drag forces were appeared to be functions of the flow incidence angle α and the turbine azimuthal angle θ. The lift is given as:

$$CL = C_y[\cos(\theta+\alpha)] - C_x[\sin(\theta+\alpha)] \quad (11)$$

which is the force acting perpendicularly to the flow direction.

And the drag as:

$$CD = C_y[\sin(\theta+\alpha)] + C_x[\cos(\theta+\alpha)] \quad (12)$$

which is the force performing opposite to the flow direction.

with $C_x = \frac{F_x}{1/2\rho c W^2}$ and $C_y = \frac{F_y}{1/2\rho c W^2}$ where F_x and F_y are the forces acting along the x and y axis, correspondingly and c is the blade cord.

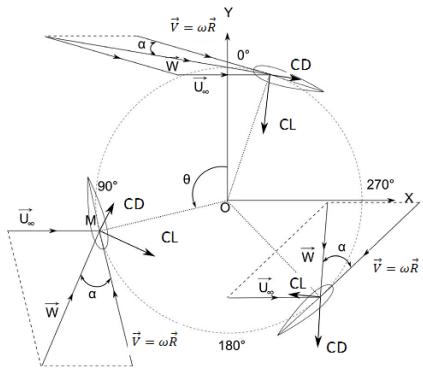

Figure 1. Forces and velocities in a VATT

3. SOLVER

The Navier-Stokes equations are stated as:

$$\rho\frac{\partial\vec{v}}{\partial t} = \vec{F} - \nabla p + \mu\nabla^2\vec{v} \quad (13)$$

where the equation of continuity is given by:

$$\nabla\vec{v} = 0 \quad (14)$$

where ρ is the fluid density, $\vec{v}$ is the velocity vector, t is the time, $\vec{F}$ is the fluid inertia volume force, p is the pressure and μ is the dynamic viscosity.

The realizable $k-\varepsilon$ turbulence model is used in the present work in fact it indicates a great consistency between the experiments and the present CFD solver.

The present simulations are achieved by using Ansys-Fluent 15.0. The SIMPLE algorithm is used for the pressure–velocity coupling. All transport equations are discretized using the third-order MUSCL convective scheme. The equations of blades deflection and that of all instantaneous forces are

integrated in a user-defined function (UDF).

4. KINEMATICS OF FLEXIBLE BLADES

The proposed blade is a NACA 0010 airfoil subjected to a rotation motion and a prescribed camber deformation (Fig.2, 3, 4). The deformation frequency can be quantified relatively to the turbine axis by the parameter $zi = \omega/2\pi \cdot f^*$which represents the ratio between the frequency of rotation and that of deformation. This parameter can be also written as $zi = \frac{f}{f^*}$ where f represents the turbine rotation frequency and $f^*$is the blade deformation frequency.

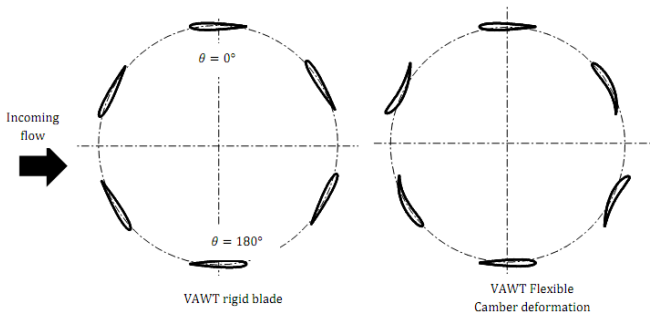

Figure 2. Photographs for the tested models over one revolution

The investigation covers the amplitude a_0/c from 0.03 to 0.2 for a fixed flapping frequency parameter zi =4.

The turbine operates at tips speed ratios between 2 and 4.7, for a constant incoming flow velocity of 3 m/s.

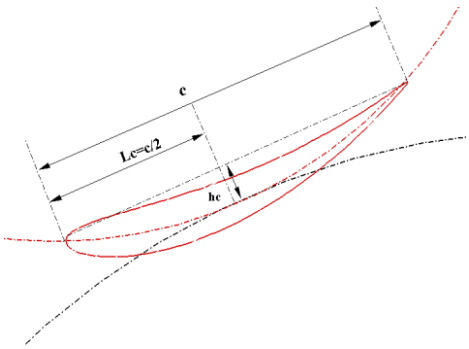

Figure 3. Schematic diagram for a deforming turbine blade

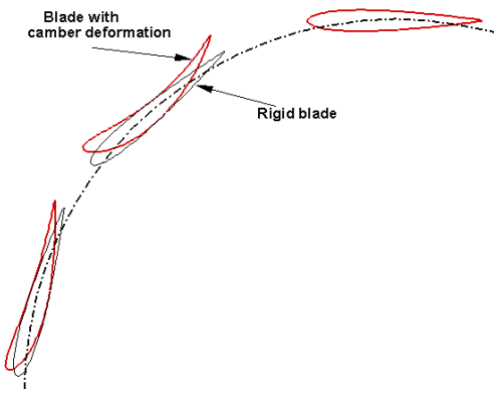

Figure 4. Flexible airfoil deformation over time (zi=4)

The profile of the deformable airfoil is given by the following equations:

Along the x axis

$$y(t) = -\frac{hc}{c}(x(y_f,t) - l_c)^2(sin(\omega_1 t + \varphi)) \quad (15)$$

And along the y axis

$$x(t) = -\frac{hc}{c}(y(x_f,t) - l_c)^2(sin(\omega_1 t + \varphi)) \quad (16)$$

where $\omega_1 = 2\pi \cdot f^*$, $\frac{hc}{c}$ denotes the camber amplitude and φ denotes the phase angle. $x(y_f,t)$ is the instantaneous airfoil position along the x axis, $y(x_f,t)$ is the instantaneous foil position along the y axis, and t is the time. x_f and y_f are the local coordinates of airfoil relative to the pitching axis. l_c is the location of the maximal camber amplitude.

Typically, for a flexible VATT the blade practices a rotating motion in addition to its flexure motion. Rotating motion is governed by the following equation:

$$\theta_t(t) = \theta_0 \sin(\omega t - \varphi) \quad (17)$$

where $\theta_t(t)$) is the instantaneous rotating angle. θ_0 is the blade initial azimuthal angle.

To achieve the anticipated blade shape, the open literature proposes a set of control systems. A mechanism similar to that suggested by Campanile [6] appears to be a practical system for a successful realization of shape-adjustable airfoil.

The present study is carried as 2D computational analysis. Previous works [1, 16-17] drawn that 2D analysis can predict correctly the most of physical phenomena occurring inside the turbine. This feature revealed that the use of 2D analysis appears to provide agreeable results.

The blades are surrounded with a finer (Fig.5) mesh in which y+ at the wall adjacent cell is around 1, consistent with a cell size of $25\mu\,m$.The mesh deformation is achieved via a Remeshing method with a deformable adjacent boundary layer (Fig.5). The dynamic mesh parameters are listed in table 1.

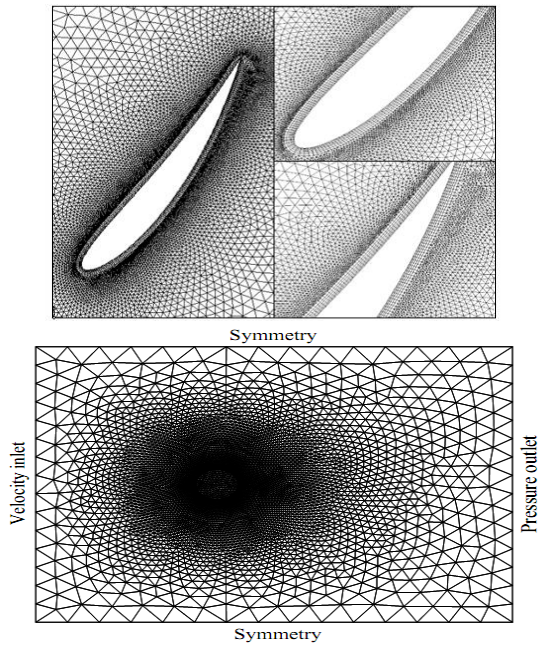

Figure 5. Simulation domain and boundary conditions

6. RESULTS

6.1. Model validation

As a standard step, the employed solver including the mesh and the numerical method should be validated with the existing literature. The work of Miao [15] is selected as a validation case study. In fact, this work examines seriously the ability of the present solver to process a combined deflection plunging problem. Fig.7 shows the variation of instantaneous drag coefficient for a reduced frequency $\frac{2\pi fc}{U_\infty} = k = 2$,non-dimensional plunge amplitude $h_0 = 0.4$, and Reynolds number $Re = 10^4$. Fig.6 indicates that the results produced by a the current solver with a time step equal to 1000/cycle match accurately the results of Miao [15]. Furthermore, a mesh size dependence test (Fig.7) confirms that a grid contains about 142.000 cells can predict correctly the momentum coefficient and the fluid fields, this grid is used for all simulations cases. The periodic solutions are achieved typically after three to four turbine cycles.

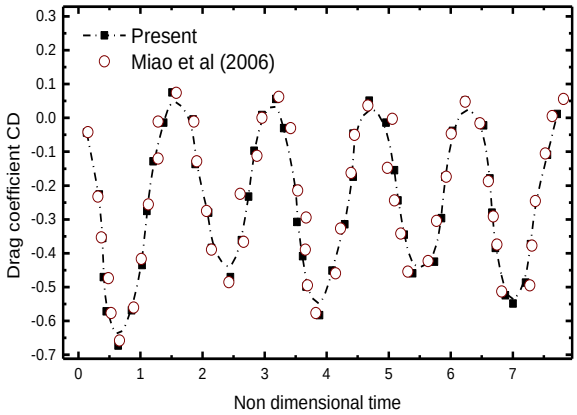

Figure 6. Validation of computational model, compared to publish results

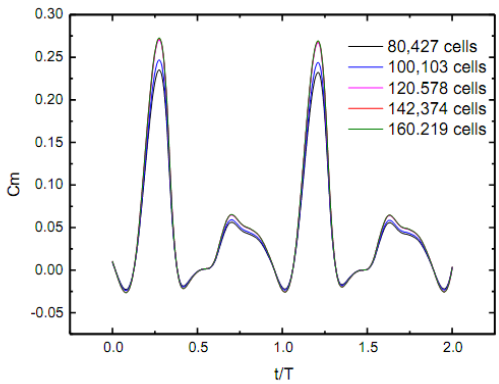

Figure 7. Instantaneous moment coefficients (grid dependent test)

6.2. Mechanism of the VATT performance improvement

To examine the turbine behavior in the presence of flexible blades, much deeper examinations of torque and lift forces behaviors are necessary. To this end, a comparison between original case and a controlled case is carried out. Fig. 8 displays the evolution of C_l , C_D and C_m over one turbine revolution. As revealed the Fig. 8(a) and (b), with the flexible blades, the quantities Cl, and Cm, display higher peaks values and they still have the same tendency as the rigid blades. Typically, the increase of C_D in the controlled case appears to have a negative contribution in the overall extracted power. However the higher increase in C_l can clearly cover this loss, so the total extracted power still evidently improved. This suggests that an appropriate flow control technique should increases C_m by increasing C_l with an acceptable increase in C_D.

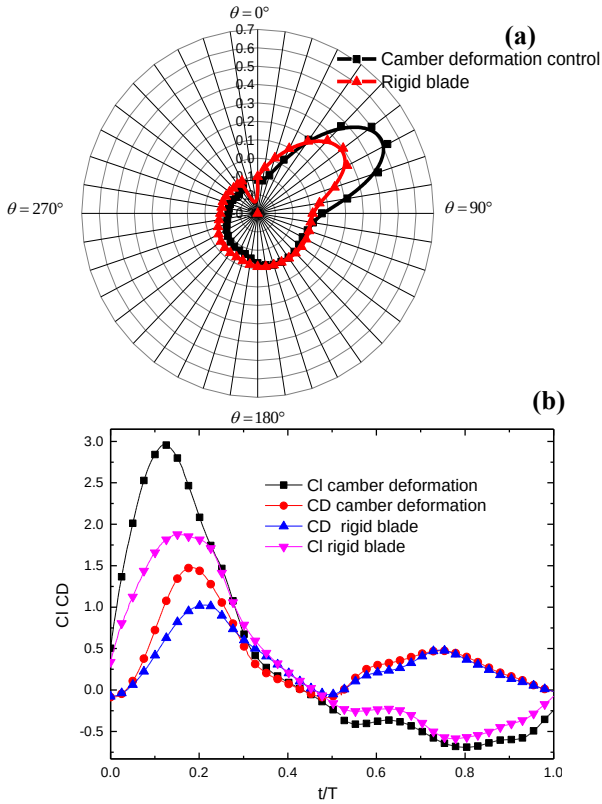

Figure 8. Comparison of (a) instantaneous moment coefficients and (b) instantaneous blade lift and drag coefficients against time for different blade turbines

The camber deformation can be considered as a deflection of the trailing edge and a deflection of the leading edge; which controls the flow angle of attack and therefore the LEV time of growth, also it is able to modify the size and strength of the LEV. Fig.9. illustrates the pressure contours for the rigid blade and for the flexible blade for an azimuthal position $\theta = 45°$. It can be seen that a significant pressure difference occurs near the leading edge between the original and the controlled turbine. The higher negative value is displayed for the controlled flexible turbine; this is attributed to the boosting of the size and the strength of LEV, which ensures suction's zones that in turn, improve the lift and the rotor torque.

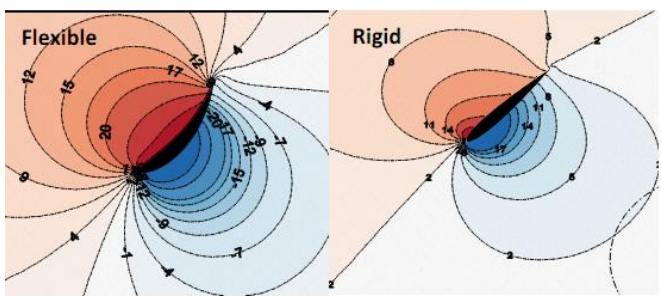

Figure 9. Comparison between blade surface pressure distributions at λ = 1.4 with a0/c=0.1 zi=4

7. EFFECT OF OSCILLATING AMPLITUDE ON THE OUTPUT POWER

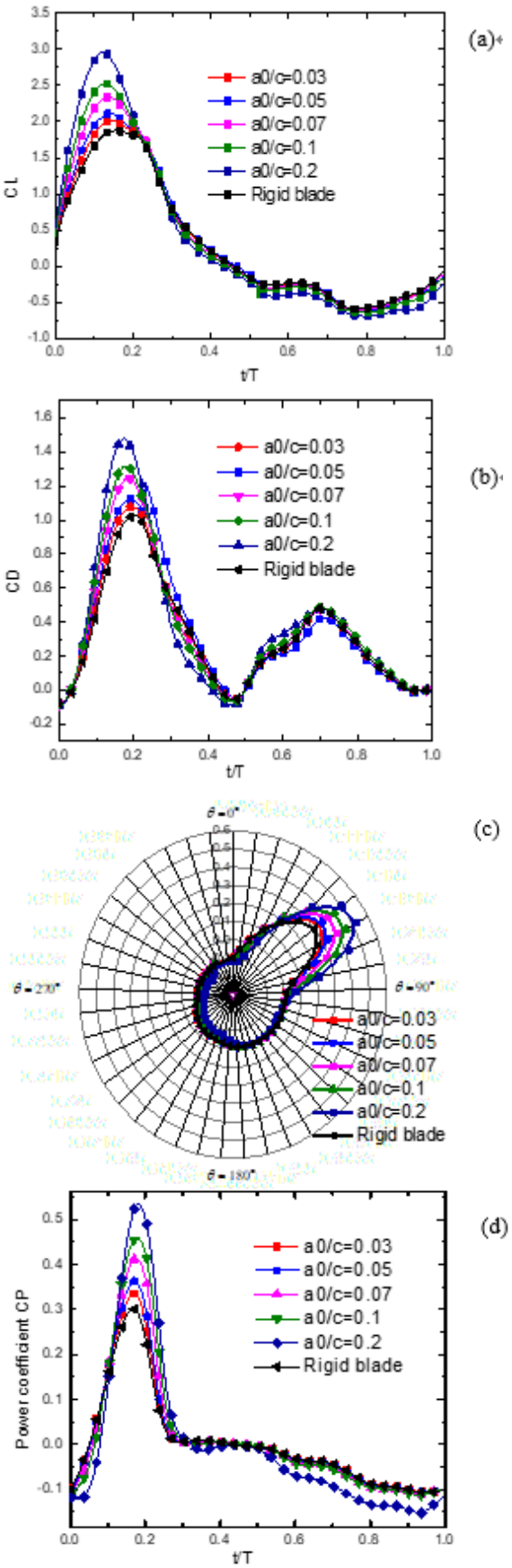

Figure 10. (a) Instantaneous lift coefficient. (b) Instantaneous drag coefficient. (c) Instantaneous blade moment coefficient versus θ. (d) Instantaneous power coefficient

In this section, the effect of oscillating amplitude on the aerodynamics forces behavior is considered. A detailed examination of the instantaneous lift, drag and torque forces is carrying out. Furthermore the instantaneous power coefficients are followed during one revolution in order to highlight the contribution of each coefficient in the system overall efficiency.

Fig.10 displays comparisons between the aerodynamic forces for the baseline case, and the controlled cases with different oscillating amplitudes.

According to Fig. 10(a), for the original case the lift coefficient indicates one peak at the upwind stroke. The peak is about 2 consistent with azimuthal position $\theta = 90°$at $t/T = 0.25$ where the LEV is fully developed. It is seen moreover that the case with an oscillating amplitude a0/c=0.2. can produce the largest peak values of C_l, the $C_l$increases from 2 to 3 relative to the original case and this is attributed to the correction of the pressure distribution. The same C_l behavior is recorded in all cases nonetheless with lower peaks. In Fig.10 (b) by using an oscillating amplitude a0/c=0.2, the drag peak increases from 1 to 1.5 relative to the baseline case. This behavior is attributed to the large wake that appears downstream the blades. The large C_l is furthermore interpreted as a peak appears clearly in the two quantities cm and C_P. For all tested cases, the turbine performance is improved as compared to the original case due to the positive contribution of deflection. Fig.10 draws also that the turbine first quarter is the zone were the most of energy is harvested.

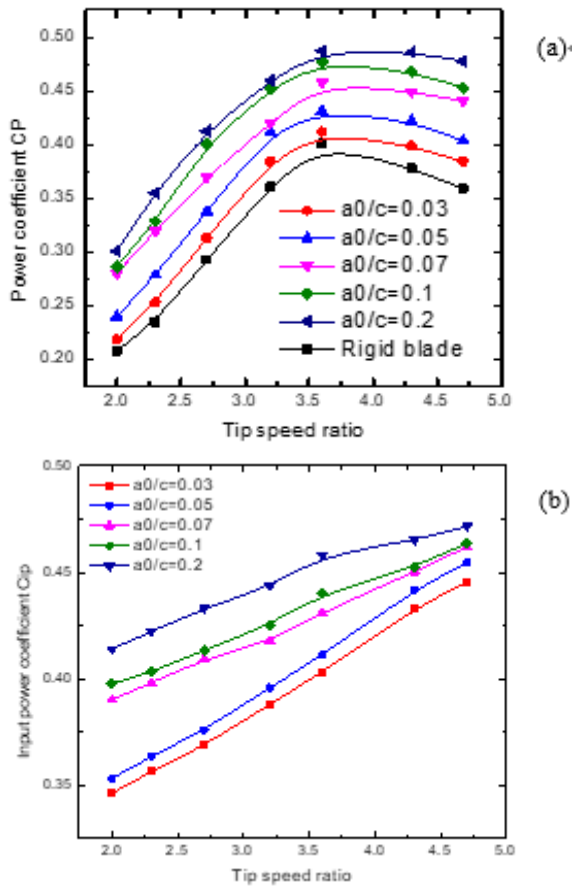

Figure 11. (a) Time-averaged power coefficient versus λ.(b) Time-averaged input power coefficient versus λ for $zi = 4$

Fig 10 (d) indicates that C_P increases from 0.3 to 0.51 for the best control condition. The power extraction plots are

directly correlated to the vorticity and pressure distribution around the blade. The effect of the LEV physical size on the total circulation over the suction surfaces explains the difference between rigid and flexible blades. Fig.11 (a) and (b) represent the variation of the mean power coefficient C_P and the input power required to deform the blades for the aforementioned cases. It can be seen that the higher C_P values are recorded at a0/c=0.2.

8. CONCLUSION

Blade shape for a VATT has a large effect on the turbine efficiency, which is primarily attributed to the nature of the interaction between the blade and the detached LEV vortex. The control and the manipulation of this expected interaction is the solution for an efficient model of VATT. As the turbine rotates, the blade can interact with the vortices generated by the blade itself or by previous blades. The ability of the blade to change its shape and therefore the flow structure interaction during the turbine rotation can produce significant improvements. The change in the blade camber line gives rise to a typical larger horizontal surface where the LEV is expected to act on. Moreover, this correction is able also to alter the flow angle of attacks and therefore the leading edge vortex time of formation, which results in an improved lift and power extraction. Computational results indicate that this strategy of control indeed enhance the VATT performance. For a tip speed ratio λ=3.5, a frequency zi=4, and a camber amplitude a0/c=0.2; the power coefficient (CP) rises about 20 % relative to the original turbine.

REFERENCES

[1] Amet E, Maître T, Pellone C, Achard JL. (2009). 2D numerical simulations of blade–vortex interaction in a Darrieus turbine. J. Fluids Eng. 131(11): 111103. https://doi.org/10.1115/1.4000258

[2] Anderson JM, Streitlien K, Barrett DS, Triantafyllou MS. (1998). Oscillating foils of high propulsive efficiency. J Fluid Mech. 360: 41-72.

[3] Beem HR, Rival DE, Triantafyllou MS. (2012). On the stabilization of leading-edge vortices with span wise flow. Exp. Fluids 52: 511-7.

[4] Bouzaher MT, Hadid M, Derfouf S.E (2017). Flow control for the vertical axis wind turbine by means of Flapping Flexible foils. J Braz. Soc. Mech. Sci. Eng. 39: 457.

[5] Bouzaher MT, Hadid M. (2017). Numerical investigation of a vertical axis tidal turbine with deforming blades. Arab J Sci Eng 42: 2167.

[6] Campanile LF. (2007). Modal synthesis of flexible mechanisms for airfoil shape control. J Int Mater Syst Struct 19: 7: 779-789.

[7] Heathcote S, Wang Z, Gursul I. (2008). Effect of spanwise flexibility on flapping wing propulsion. J. Fluids Struct 24: 183-99.

[8] Hoke CM, Young J. Lai JCS. (2015). Effects of time-varying camber deformation on flapping foil propulsion and power extraction. Journal of Fluids and Structures 56: 152–176.

[9] Hoogedoorn E, Jacobs GB, Beyene A. (2010). Aero-elastic behavior of a flexible blade for wind turbine application: A 2D computational study. Energy 35(2): 778–85.

[10] Jie W, Chen L, Yang SC, Zhao N. (2015). Influence of a flexible tail on the performance of a foil hovering near the ground: Numerical investigation. European Journal of Mechanics B/Fluids 52: 85–96.

[11] Liu W, Xiao Q, Cheng F. (2013). A bio-inspired study on tidal energy extraction with Flexible lapping wings. Bioinspir.Biomim. 2013Sep; 8(3): 036011.

[12] Lee AT, Flay RGJ. (1999). Compliant blades for wind turbines. Trans Inst Prof Eng NZ: Electr/Mech/Chem Eng. Sect 26(1): 7.

[13] Liu WY, Zhang X, Liu XF, Gong JX. (2010). Bionic design and performance study for flexible blades of wind turbine. J Mach Des 5: 7–10

[14] Liu W, Xiao Q. (2015). Investigation on Darrieus type straight blade vertical axis wind turbine with flexible blade. Ocean Engineering 110: 339–356

[15] Miao JM, Ho MH. (2006). Effect of flexure on aerodynamic propulsive efficiency of flapping flexible airfoil. Journal of Fluids and Structures 22: 401-419.

[16] Maître T, Amet E, Pellone C. (2013). Modeling of the low in a Darrieus water turbine: wall grid reinement analysis and comparison with experiments. Renew Energy 51: 497-512

[17] Nabavi Y. (2008). Numerical study of the duct shape effect on the performance of a ducted vertical axis tidal turbine. PhD thesis, University of British Columbia, Vancouver, Canada.

[18] Read DA, Hover FS, Triantafyllou MS. (2003). Forces on oscillating foils for propulsion and maneuvering. J Fluids Struct 17: 163-83.

[19] Tuyen QL, Jin HK. (2015). Effect of hydrofoil flexibility on the power extraction of a flapping tidal generator via two- and three-dimensional flow simulations. Renewable Energy 80: 275-285

[20] Wang Y, Sun XJ, Dong XH, Zhu B, Huang DG, Zheng ZQ. (2016). Numerical investigation on aerodynamic performance of a novel vertical axis wind turbine with adaptive blades. Energy Conversion and Management 108: 275–286.